IOPscience iopscience.iop.org

Home Search Collections Journals About Contact us My IOPscience

Effects of uniaxial stress on the $^2E \rightarrow {}^2T_2$ absorption lines of $GaP : Ti^{3+}$ and the nature of the Jahn-Teller coupling

This article has been downloaded from IOPscience. Please scroll down to see the full text article.

1998 J. Phys.: Condens. Matter 10 3367

(http://iopscience.iop.org/0953-8984/10/15/014)

View the table of contents for this issue, or go to the journal homepage for more

Download details:
IP Address: 171.66.16.209
The article was downloaded on 14/05/2010 at 12:56

Please note that terms and conditions apply.

J. Phys.: Condens. Matter **10** (1998) 3367–3386. Printed in the UK PII: S0953-8984(98)86171-7

Effects of uniaxial stress on the $^2E \rightarrow {}^2T_2$ absorption lines of GaP:Ti^{3+} and the nature of the Jahn–Teller coupling

A M Al-Shaikh†‖, Q C Qiu†, P Roura‡¶, W Ulrici§, B Clerjaud‡, C A Bates† and J L Dunn†

† Department of Physics, The University of Nottingham, Nottingham NG7 2RD, UK

‡ Laboratoire d'Optique des Solides, Université Pierre et Marie Curie, Case 80, F-75252 Paris Cédex 05, France

§ Paul-Drude-Institut für Festkörperelektronik, Hausvogteiplatz 5–7, 10117-Berlin, Germany

Received 18 July 1997, in final form 29 January 1998

Abstract. Experiments showing the effects of uniaxial stress on the structure of the zero-phonon line (ZPL) obtained in the optical absorption spectrum from a Ti^{3+} ion in GaP are described and interpreted using a new theoretical model. It is found that the components of the ZPL are split when the stress is applied along the ⟨001⟩, ⟨111⟩ and ⟨110⟩ axes. These results together with the spectra observed without applied stress, show that previous energy level diagrams for this centre cannot be correct. A vibronic model is used to describe this system which includes coupling to e modes in the ^2E ground states, to both e and t_2 modes in the excited $^2T_2$ excited states and to t_2 modes between ^2E and $^2T_2$. The model is shown also to give a good explanation of the published Zeeman data obtained from photoluminescence measurements as well as the new uniaxial stress data presented here. A brief discussion is given of the type of Jahn–Teller effect operational in this system emphasizing that it is not necessarily of the orthorhombic $T \otimes (e + t_2)$ type in the excited state.

1. Introduction

Impurities continue to play a dominant rôle in the search for superior materials for use as electronic and optoelectronic devices. One of the simplest impurities to understand would appear to be titanium in the Ti^{3+} form when it substitutes for a host atom, as it contains a single 3d electron localized around the impurity centre. However, this is clearly not the case as demonstrated from the conflicting models which have been presented in the literature for the Ti^{3+} impurity in the III–V semiconductors GaAs, GaP and InP over the last ten years. During this period, a variety of experimental techniques have been used in attempts to elucidate the facts but their interpretation is hindered by the lack of adequate theory to explain some of the observed properties. The aim of this paper is to describe some new experiments undertaken on the GaP:Ti^{3+} system and some advancements in the theory which together enable a satisfactory model to be obtained for this system. The results obtained clearly show the need to be careful in attributions of particular properties of defects in device material to specific impurities.

It has been established that the Ti ion substitutes for the III site in the three hosts mentioned above and that it forms both a deep donor Ti^{3+}/Ti^{4+} level and a deep acceptor

‖ Now at: Physics Department, College of Science, University of Mosul, Mosul, Iraq.

¶ Permanent address: Dipartament d'Enginyeria Industrial, Universitat de Girona, 17071 Girona, Spain.

0953-8984/98/153367+20$19.50 © 1998 IOP Publishing Ltd

Ti^{2+}/Ti^{3+} level within the band gap [1–9] in both GaAs and GaP. By carefully controlling the other impurities, it has been possible to isolate those properties associated with Ti^{3+} ions alone. In a tetrahedral environment arising from the four nearest-neighbour arsenic or phosphorus atoms, the Ti^{3+} impurity has a ^2E ground state and a $^2T_2$ excited state. It can thus be investigated spectroscopically.

Electron paramagnetic resonance (EPR) experiments on Ti^{3+} in GaP [10, 11] and in GaAs [12] have suggested that the orbital doublet (^2E) ground state undergoes a weak-to-medium $E \otimes e$ Jahn–Teller (JT) coupling. This is inferred by a line-shape analysis of the broad EPR line at low temperatures with the Huang–Rhys factor $S_e \approx 2$. Information on the excited $^2T_2$ state is available from different optical absorption (OA) and photoluminescence (PL) experiments which involve also the ground state. At low temperatures, the OA spectra in GaAs and InP are characterized by two sharp peaks of the ^2E–$^2T_2$ zero-phonon line (ZPL) located at 4565.5 cm^{-1} and 4589.4 cm^{-1} in GaAs [1, 7, 14–16] and at 4409.4 cm^{-1} and 4437.0 cm^{-1} in InP [1, 7, 15]. In GaP, the same features have been observed; however, the first peak was found to be split into two components located at 4873.0 cm^{-1} and 4876.3 cm^{-1} [17]. Also, the second peak, at 4903.0 cm^{-1}, has a full width at half-maximum (FWHM) which is an order of magnitude ($\approx$8 cm^{-1}) larger than that of the two components of the first peak. Similarly, it has also been noted that the second peaks of the OA spectra in the cases of GaAs and InP hosts are also again much wider than the corresponding first peaks in these hosts. These measurements clearly suggest that the nature of the electronic transitions associated with the first and second peaks in all three hosts are different. Additional information has been obtained from studies of the effects of a magnetic field; Zeeman experiments have been carried out on the first peak by PL in GaP [18] and by OA in both GaAs [14] and InP [15].

Agreement on the origin of the peaks in the ZPLs in all three hosts appeared to have been reached in the papers cited above including the important characteristic that one of the observed Zeeman lines in GaP:Ti^{3+} was virtually field independent. The two absorption lines were assigned to the transitions from the $\Gamma_8(^2E)$ ground state to the Γ_8 and Γ_7 components of the $^2T_2$ excited state which are separated by an amount $3K\lambda/2$ from the spin–orbit interaction where λ is the free-ion spin–orbit coupling constant (159 cm^{-1}) and the factor K is equal to unity in a crystal-field model. However, the measured value (28 cm^{-1}) of the splitting of the excited state in all three hosts was found to be much smaller than the value of $3\lambda/2$ (231 cm^{-1}). This difference was explained by taking $K = 0.12$ and attributing the origin of the quenching of the spin–orbit interaction to the Jahn–Teller (JT) effect. The smaller splitting of 3.3 cm^{-1} observed in the first two peaks in GaP was explained by the presence of a non-cubic distortion, although its origin remained unclarified [18].

Meanwhile, Zeeman experiments on the OA ZPLs in InP:Ti^{3+} [15] gave results which conflicted with this model. Instead, the measurements suggested that the second (broader) peak was unlikely to correspond to the $\Gamma_8(^2E) \rightarrow \Gamma_7(^2T_2)$ transition. Furthermore, the value of 0.12 deduced above for K is an order of magnitude larger than that usually associated with deep-level impurity ions in III–V semiconductors (see [19], for example).

In order to clarify the details of the simultaneous action of spin–orbit coupling and the vibronic coupling on the excited $^2T_2$ state in such systems, the behaviour of the absorption lines under uniaxial stress has been investigated for one of the hosts. This paper describes such experiments carried out on the GaP:Ti^{3+} system. It is shown that the results require a reinterpretation of the assignment of the Ti^{3+}-related absorption lines for this system. A new theoretical model is developed which takes into account both the spin–orbit coupling and the vibronic coupling of the T_2 orbital excited states to the e and t_2 modes (including second-order JT effects) as well as 'strain'-like effects. This model in which the splitting within

the excited $^2T_2$ vibronic states is much less than the value of 28 cm^{-1} quoted above will be shown to give a good description of the stress-induced shifts, splittings and polarization behaviour of the absorption lines. Thus $3\lambda/2$ is no longer taken to be 28 cm^{-1}; instead, the latter level is taken to be the first excited vibronic level of the system.

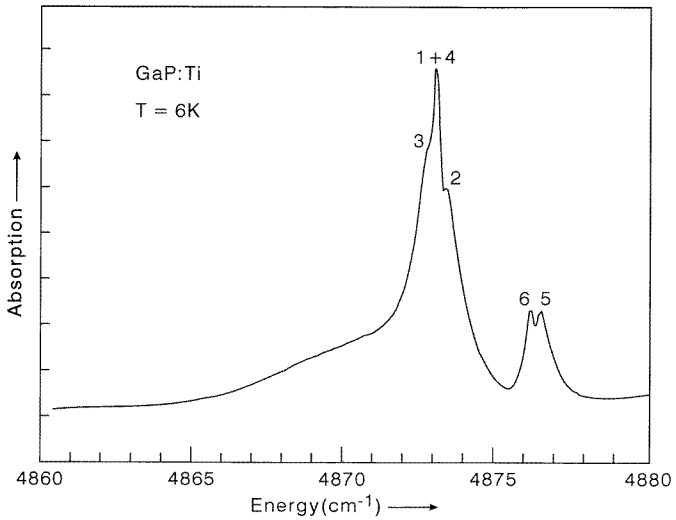

Figure 1. Absorption spectrum of GaP:Ti measured at $T = 6$ K. The numbers indicate the $^2E \rightarrow {}^2T_2$ transitions of Ti^{3+}_{Ga} according to the energy level scheme of figure 4.

Table 1. The relative strengths of the absorption lines 1 to 6 as described in the spectra of figures 2 and 3. Key: ×: line present; ⊗: line present but weaker (<20%); △: line weak (<20%) in both polarizations; ○: line absent; $\boldsymbol{E}$: electric vector of the absorbed light; $\boldsymbol{\sigma}$: pressure.

		1	2	3	4	5	6
$\boldsymbol{\sigma} \parallel \langle 001 \rangle$	$E \parallel \boldsymbol{\sigma}$	⊗	×	○	○	×	△
	$E \perp \boldsymbol{\sigma}$	×	×	×	×	○	△
$\boldsymbol{\sigma} \parallel \langle 111 \rangle$	$E \parallel \boldsymbol{\sigma}$	×	×	×	×	○	○
	$E \perp \boldsymbol{\sigma}$	×	×	×	×	×	×

The reassignment of the level at 28 cm^{-1} is the fundamental difference between existing models of this centre and that described here. As stated above, the reasons for this change are based on the differences between the *experimentally observed* linewidths and shapes of the observed transitions under zero stress. A second and perhaps even more important experimental factor is that the observed splittings of the first peak of the ZPL generated by uniaxial stress cannot be explained with existing models as six components are seen rather than the four which would arise according to existing models. A vibronic level at 28 cm^{-1} is not unexpected on physical grounds. It could be typically an inversion level in a strongly coupled JT ion or another vibronic level containing one-phonon excitation; it is impossible to be more definitive than this at the present time. However, the origin is unimportant for setting up a model.

In addition to providing an acceptable explanation of the stress data, the model will be shown also to give a consistent reinterpretation of the earlier Zeeman experiments on the lines in PL. Although details are not given in this paper, the same basic model can be shown to account for the observed properties of the Ti^{3+} ion in GaAs and InP (although obviously the values of the parameters will be different).

Finally, as the Ti^{3+} ion is the simplest of the transition metal impurity ions, it provides an ideal system in which to study the JT effect when both e and t_2 couplings are present.

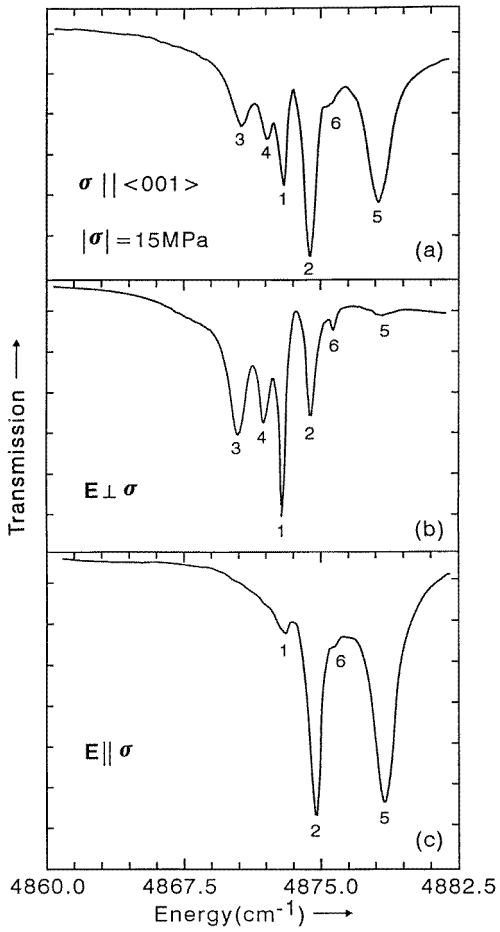

Figure 2. The transmission spectra due to the $^2E \rightarrow {}^2T_2$ transitions 1 to 6 (see figure 4) of GaP:Ti^{3+} measured at $T = 6$ K with uniaxial stress $\boldsymbol{\sigma}$ along $\langle 001 \rangle$ (resolution 0.2 cm^{-1}). (a) Measured with unpolarized light, (b) measured with polarized light and the electric field $\boldsymbol{E}$ of the absorbed light perpendicular to the stress direction $\boldsymbol{\sigma}$, (c) measured with polarized light and $\boldsymbol{E}$ parallel to $\boldsymbol{\sigma}$.

2. Experimental details and results

The titanium-doped GaP samples investigated were taken from the same LEC-grown boule as was used in earlier investigations; they are n-type semi-insulating with the Fermi level

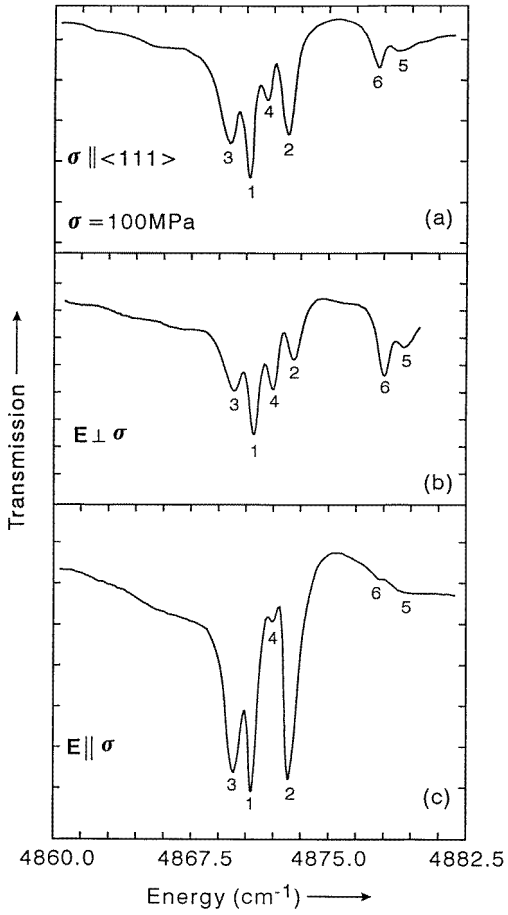

Figure 3. The transmission spectra due to the $^2E \rightarrow {}^2T_2$ transitions 1 to 6 (see figure 4) of GaP:Ti^{3+} measured at $T = 6$ K with uniaxial stress $\boldsymbol{\sigma}$ along $\langle 111 \rangle$ (resolution 0.2 cm^{-1}). (a) Measured with unpolarized light, (b) measured with polarized light and the electric field $\boldsymbol{E}$ of the absorbed light perpendicular to the stress direction $\boldsymbol{\sigma}$, (c) measured with polarized light and $\boldsymbol{E}$ parallel to $\boldsymbol{\sigma}$.

pinned by the $Ti^{2+}_{Ga}/Ti^{3+}_{Ga}$ level at $E_c - 0.5$ eV (E1 samples; cf. [17]). For measuring the OA, three samples were each cut with dimensions $10 \times 4 \times 2$ mm^3 but with the 10 mm axes parallel to either the $\langle 001 \rangle$, $\langle 111 \rangle$ or $\langle 110 \rangle$ directions respectively. The 10×2 mm^2 faces were polished so that the absorbing thickness was 4 mm. The OA was measured by Fourier-transform spectroscopy using a BOMEM DA 3.01 interferometer equipped with a cooled InSb detector and a CaF_2 beam splitter. The resolution in all of the experiments was 0.2 cm^{-1}. The samples were mounted in an uniaxial compressive stress system inserted into an Oxford Instruments CF 204 continuous-flow cryostat. The experiments were performed at temperatures close to 6 K.

Figure 1 shows the absorption spectrum of GaP:Ti in the region of the known two sharp peaks at 4873 cm^{-1} and 4876.3 cm^{-1} arising from the $^2E \rightarrow {}^2T_2$ transition of Ti^{3+}. This spectrum measured with this high resolution and without applied stress, reveals that the ZPLs at 4873 cm^{-1} and 4876 cm^{-1} consist at least of three and two lines respectively. The

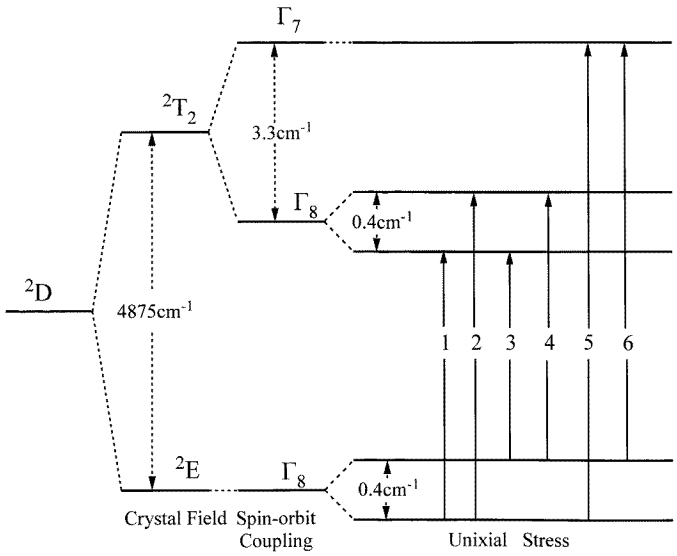

Figure 4. The energy level scheme of Ti^{3+}_{Ga} in GaP in zero applied uniaxial stress. The arrows marked by 1 to 6 indicate the optical absorption transitions seen in the spectra of figures 1 to 3.

broad underlying absorption seen in figure 1 is due to the $^3A_2 \rightarrow {}^3T_1$ transition of the Ti^{2+} ion which is also present in the samples (cf. figure 2 in [17]).

The shifts and splittings of the absorption lines shown in figure 1 under uniaxial stress σ, with σ having values up to 100 MPa, have been investigated for $\boldsymbol{\sigma}$ along $\langle 001\rangle$, $\langle 111\rangle$ and $\langle 110\rangle$ successively. Parts (a) of figure 2 and figure 3 show the spectra measured with unpolarized light and the stress applied along $\langle 001\rangle$ and $\langle 111\rangle$ respectively. Parts (b) and (c) of figure 2 and figure 3 show the spectra measured with polarized light where parts (b) are the spectra for the electric field $\boldsymbol{E}$ of the absorbed light perpendicular to $\boldsymbol{\sigma}$ and parts (c) for $\boldsymbol{E}$ parallel to $\boldsymbol{\sigma}$. As can be seen, quite pronounced polarization effects occur for both stress directions. The relative intensities of the transitions are summarized in table 1.

The spectra measured under stress clearly indicate that a total of six absorption lines exist. Analysing the positions of the lines at zero and low stresses, the schematic energy level scheme shown in figure 4 has been derived to describe the electronic $^2E \rightarrow {}^2T_2$ transitions within a Ti^{3+}_{Ga} ion. These transitions are labelled by 1 to 6 in figure 4. In particular, this level scheme, which is totally different from that usually assumed in the literature (see references [1–17]), shows that:

(i) the spin–orbit splitting of the $^2T_2$ excited state into the Γ_8 and Γ_7 states amounts to only 3.3 cm^{-1}, and

(ii) both the $\Gamma_8(^2E)$ ground state and the $\Gamma_8(^2T_2)$ excited state are already split at zero stress by about 0.4 cm^{-1}.

The almost equal splitting of the two Γ_8 states implies that transitions 1 and 4 are at the same energy at zero stress, so only five lines can actually be observed (see figure 1). The observation of all six lines in high stresses shows that the broader line at 4903 cm^{-1} is not a purely electronic transition but more probably vibronic in nature.

Figures 5 to 7 show the dependence of the positions of the absorption lines 1 to 6 on the uniaxial stress applied along the directions $\langle 001\rangle$, $\langle 111\rangle$ and $\langle 110\rangle$ respectively. As can

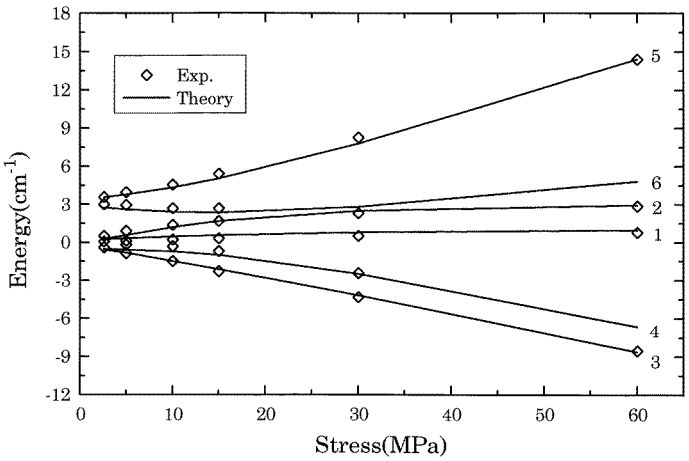

Figure 5. The effects of uniaxial stress on the absorption lines 1 to 6 for GaP:Ti^{3+} for $\boldsymbol{\sigma}$ applied along the ⟨001⟩ direction. The diamonds are the measured line positions with $\Delta E = 0$ at 4873.0 cm^{-1}. The curves are fits to the Jahn–Teller model with the parameters given in section 4.

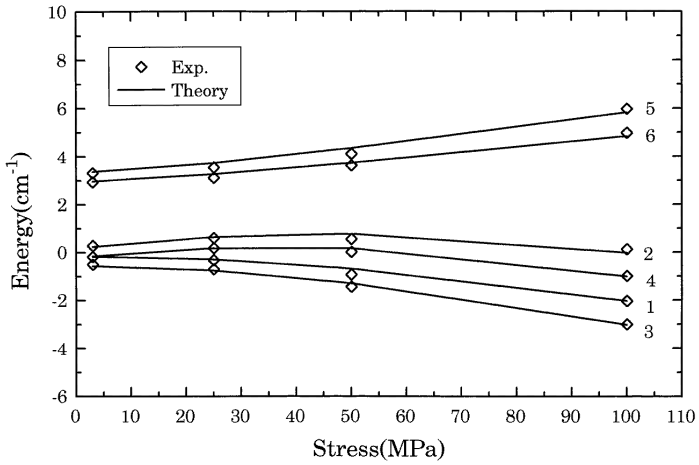

Figure 6. The effects of uniaxial stress on the absorption lines 1 to 6 for GaP:Ti^{3+} for $\boldsymbol{\sigma}$ applied along the ⟨111⟩ direction. The diamonds are the measured line positions with $\Delta E = 0$ at 4873.0 cm^{-1}. The curves are fits to the Jahn–Teller model with the parameters given in section 4.

be seen, the effect of stress is much larger for $\boldsymbol{\sigma}$ along ⟨001⟩ compared with $\boldsymbol{\sigma}$ along ⟨111⟩ but that it is also significant for $\boldsymbol{\sigma}$ along ⟨110⟩.

For comparison, figure 8 shows the absorption line at 4565.5 cm^{-1} due to the $^2\mathrm{E} \rightarrow {}^2\mathrm{T}_2$ transition of $\mathrm{Ti}^{3+}_{\mathrm{Ga}}$ in GaAs measured with high resolution on a sample investigated previously [14]. Obviously this line consists of two components separated by ∼0.2 cm^{-1}. This result suggests that the spin–orbit splitting of the $^2\mathrm{T}_2$ state amounts to only 0.2 cm^{-1} in GaAs:Ti^{3+} and that the Γ_8 states are not split without an external perturbation. It is therefore assumed that the second peak in GaAs and InP is also vibronic in nature. Thus a more detailed analysis of these systems is required, taking the JT effect into account in a general way.

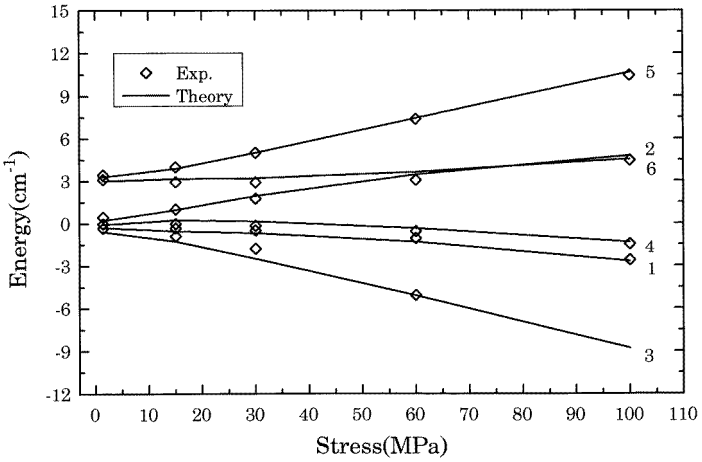

Figure 7. The effects of uniaxial stress on the absorption lines 1 to 6 for GaP:Ti^{3+} for σ applied along the ⟨110⟩ direction. The diamonds are the measured line positions with $\Delta E = 0$ at 4873.0 cm^{-1}. The curves are fits to the Jahn–Teller model with the parameters given in section 4.

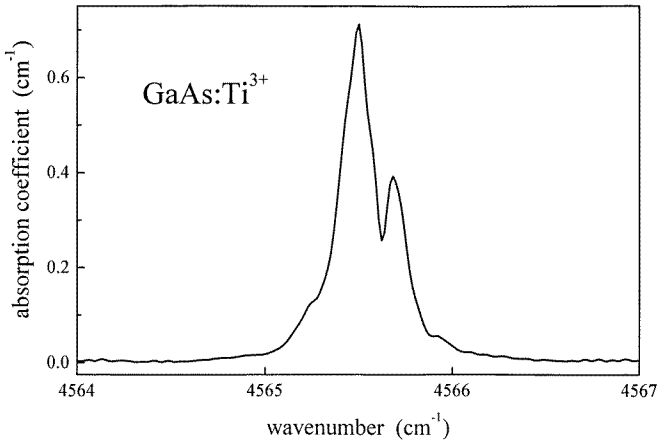

Figure 8. The optical absorption spectrum of GaAs:Ti measured at $T = 6$ K with a resolution of 0.05 cm^{-1} in the region of the zero-phonon line at 4565.5 cm^{-1}. The two partly resolved lines (separation 0.19 cm^{-1}) are due to the $^2E \rightarrow {}^2T_2$ transition of Ti^{3+}_{Ga} with the $^2T_2$ state split into the Γ_8 and Γ_7 components. The weak shoulders on the wings of these lines are caused by the isotope effect of ^{46}Ti (7.9%), ^{47}Ti (7.3%), ^{49}Ti (5.5%) and ^{50}Ti (5.3%); the numbers in brackets are the natural abundances.

3. The Jahn–Teller model for Ti^{3+} in GaP

3.1. The Jahn–Teller effect

It is usual to simplify the description of the lattice by replacing it by a cluster which consists of the paramagnetic ion and its nearest neighbours only. This is known as the cluster model. We assume that the largest perturbation is the crystal field followed by the ion–lattice interaction $\mathcal{H}_{int}$. Only e modes can be coupled to the orbital doublet but the

orbital triplet can couple to the e- and two t_2-type vibrations. From a theoretical point of view, it is impossible to say which of the e- and two t_2-type vibrations are more strongly coupled in the orbital triplet. However, from the above uniaxial stress experiments, it appears that tetragonal (e) uniaxial stress has the main effect on the $^2T_2$ state but also that trigonal (t_2) uniaxial stress does have an effect, so we must infer that both the e- and t_2-mode couplings are significant without the system being necessarily orthorhombic. The influence of the coupling to t_2 modes of the $^2T_2$ is also revealed by the triple-peaked line-shape of the broad $^2E \rightarrow {}^2T_2$ absorption band observed for all three hosts (see figures 2 and 3 in [1] and figure 3 in [10]). The structure due to the various titanium isotopes observed in figure 8 confirms, in the case of GaAs, the importance of the coupling to t_2 modes as e modes do not induce a motion of the titanium ions. It seems appropriate, therefore, to model the orbital triplet by an effective Hamiltonian which allows for coupling to the e and the two t_2 modes without any other restriction.

The Hamiltonian for the $^2T_2$ orbital triplet of the Ti^{3+} ion at a site of symmetry T_d can be written as

$$\mathcal{H} = E_O + \mathcal{H}_{int} + \mathcal{H}_{\text{cluster}} + V \tag{3.1}$$

where E_O is the energy of the orbital triplet, $\mathcal{H}_{\text{cluster}}$ is the total elastic and kinetic energy of the cluster and V represents any perturbations such as spin–orbit coupling, the Zeeman term, the stress/strain etc. The vibronic coupling $\mathcal{H}_{int}$ is assumed to have the form

$$\begin{aligned}\mathcal{H}_{int} = {} & V_{\mathrm{E}}(Q_\theta E_\theta + Q_\epsilon E_\epsilon) + V_{\mathrm{T}}(Q_4 T_{yz} + Q_5 T_{zx} + Q_6 T_{xy}) \\ & + V_2(Q_7 T_{yz} + Q_8 T_{zx} + Q_9 T_{xy})\end{aligned} \tag{3.2}$$

where V_{E}, V_{T} and V_2 are the coupling constant for the e-type and the two t_2-type displacements respectively. E_θ, E_ϵ and T_{xy} are orbital operators such that

$$E_\theta = \tfrac{1}{2}[3l_z^2 - l(l+1)] \qquad E_\epsilon = \tfrac{1}{4}\sqrt{3}(l_+^2 + l_-^2) \qquad T_{xy} = \tfrac{1}{2}\sqrt{3}(l_x l_y + l_y l_x)$$

etc, where the orbital operators are written in terms of an isomorphic operator $l = 1$ and O_z is along one of the twofold $\langle 001 \rangle$ axes of the tetrahedral cluster [20].

For the ^2E orbital doublet, modelled by an isomorphic orbital operator $T = \frac{1}{2}$, equations (3.1) and (3.2) apply but with the orbital operators defined by [20]

$$\begin{aligned}E_\theta &= T_1 = \tfrac{1}{2}(|\theta\rangle\langle\theta| - |\epsilon\rangle\langle\epsilon|) \\ E_\epsilon &= T_2 = -\tfrac{1}{2}(|\theta\rangle\langle\epsilon| - |\epsilon\rangle\langle\theta|).\end{aligned} \tag{3.3}$$

The vibronic coupling $\mathcal{H}_{int}$ has the form $\mathcal{H}_{int} = V'_{\mathrm{E}}(Q_\theta T_1 + Q_\epsilon T_2)$. The eigenstates associated with both the orbital triplet and orbital doublet are necessarily vibronic in character.

So far, it has been assumed that the titanium ions substitute for gallium atoms, and the environment remains tetrahedral. However, the titanium and gallium atoms have different sizes, so such substitutions, and also the presence of other impurities, inevitably imply that the lattice will have internal strains. Thus a given titanium ion is unlikely to be at a site which has true tetrahedral symmetry, and the question arises as to the relative importance of the internal strains and their origins. In order to take strains into account, it is sufficient to use equation (3.2) again but with the variables Q_i having fixed values $\bar{Q}_i$ which change from site to site. Usually, it is not possible to predict which symmetries and magnitudes of strains are active in a given system without reference to the experimental results. Nevertheless, it is clear from our subsequent analysis of the uniaxial stress data for this system that such terms must be added here.

3.2. The effect of perturbations

It is usual to create an effective Hamiltonian $\mathcal{H}_{eff}$ to describe any perturbation V within each set of vibronic states after JT effects via $\mathcal{H}_{int}$ have been considered. Then $\mathcal{H}_{eff}$ may be obtained directly from V by multiplying the various symmetry-adapted orbital operators within V by first-order reduction factors appropriate to that symmetry and adding in appropriate second-order JT terms. The perturbations needed here to describe the experimental results are the spin–orbit coupling, the 'strain'-like terms and uniaxial stress. We consider first the $^2T_2$ vibronic excited state and then the ^2E vibronic ground state.

3.2.1. The vibronic excited state. The effective Hamiltonian is given in general by

$$\mathcal{H}^e_{eff} = \mathcal{H}^{(1)-so} + \mathcal{H}^{(2)-so} + \mathcal{H}^e_{\text{strain}} + \mathcal{H}^e_{\text{stress}} \tag{3.4}$$

where $\mathcal{H}^{(1)-so}$ and $\mathcal{H}^{(2)-so}$ are due to the spin–orbit coupling $\lambda \boldsymbol{l}\cdot\boldsymbol{S}$ within the orbital triplet where the first-order term is given by

$$\mathcal{H}^{(1)-so} = K(\mathrm{T}_1)\lambda \boldsymbol{l}\cdot\boldsymbol{S} \tag{3.5}$$

with $K(\mathrm{T}_1) = K$ in the notation used earlier. The value of the first-order reduction factor $K(\mathrm{T}_1)$ depends upon the nature and magnitude of the vibronic coupling. Neglecting the constant term, the second-order JT contributions from spin–orbit coupling are often written in the general form

$$\mathcal{H}^{(2)-so} = \lambda^2[a(\boldsymbol{l}\cdot\boldsymbol{S}) + b(\boldsymbol{l}\cdot\boldsymbol{S})^2 + c(E_\theta E^S_\theta + E^S_\epsilon E^S_\epsilon) + d(T_{yz}S_{yz} + T_{zx}S_{zx} + T_{xy}S_{xy})] \tag{3.6}$$

where E^S_θ etc is equal to E_θ etc with the l-operators replaced by S-operators. The parameters b, c and d also depend upon the nature and magnitude of the coupling. For example, their values for a $\mathrm{T}\otimes\mathrm{e}$ JT system are given in references [20] and [21] and for the $\mathrm{T}\otimes\mathrm{t}_2$ and $\mathrm{T}\otimes(\mathrm{e}+\mathrm{t}_2)$ systems in references [22] and [23] respectively. However, the form (3.6) is overspecified with parameters, as the individual terms have mixed symmetries. Thus here we take $d = 0$. We note also that the term in c does not contribute, as $S = \frac{1}{2}$ for a $^2T_2$ term. Furthermore, the spin–orbit coupling gives a term in $\boldsymbol{l}\cdot\boldsymbol{S}$ in both the first- and second-order expressions and they thus will be combined together in the term $a'(\boldsymbol{l}\cdot\boldsymbol{S})$. (A second second-order term should be added to (3.6) arising from the direct ^2E–$^2T_2$ coupling via the spin–orbit interaction. However, the form for this is exactly the same as the second-order JT contribution (3.6) but with smaller values for the coefficients. Thus henceforth we will consider that such contributions are absorbed into (3.6).)

Further simplifications in the analysis can be made as we note that it is impossible to obtain independent values for the parameters a' and b for an ion such as Ti^{3+}. (We note also that a' and b cannot be separated in intensity calculations which will be discussed later.) Thus we use instead the observed zero-stress splitting of 3.3 cm^{-1} ([18] and shown here in figure 4) for the excited $^2T_2$ vibronic state. We will denote this by E $(= -3[\frac{1}{2}a' - \frac{1}{4}b\lambda^2])$.

The remaining terms in the general effective Hamiltonian (3.4) are $\mathcal{H}^e_{\text{strain}}$, which represents the very small strain-like splitting of fixed magnitude observed experimentally, and $\mathcal{H}^e_{\text{stress}}$, which is the perturbation to represent the applied uniaxial stress. (The label e denotes the excited state.) The externally applied uniaxial stress will cause each impurity ion to experience a strain which is superimposed on the random strains already present in the crystal. The nature of the term '$\mathcal{H}^e_{\text{strain}}$' in the effective Hamiltonian is not clear at this stage. It could represent an internal 'strain' of fixed magnitude or the value of the true

random strain at the peak of the strain distribution. All we know is that, in order to describe the observed results, it is necessary to add the term

$$\mathcal{H}^{e}_{\text{strain}} = \alpha l_z^2 \tag{3.7}$$

to the effective Hamiltonian, where α is a parameter to be determined which describes the observed zero-stress splittings.

The effect of a uniaxial stress $\boldsymbol{\sigma}$ along the $\langle 001\rangle$ axis can be described by the Hamiltonian $\mathcal{H}^{e}_{\text{stress}}$ and becomes

$$\mathcal{H}^{e,\langle 001\rangle}_{\text{stress}} = A\sigma - \eta\sigma(3l_z^2 - 2) \tag{3.8}$$

where A is the hydrostatic term and η is the tetragonal stress coefficient. (As the experiments give transition and not absolute energies, we attribute the whole of the hydrostatic term to the excited states.) The effect of a stress along $\langle 111\rangle$ can be described by the Hamiltonian

$$\mathcal{H}^{e,\langle 111\rangle}_{\text{stress}} = A\sigma + \frac{2}{3\sqrt{3}}\gamma\sigma[T_{yz} + T_{zx} + T_{xy}] \tag{3.9}$$

where γ is the trigonal stress coefficient. For stress along $\langle 110\rangle$, the corresponding Hamiltonian is given by

$$\mathcal{H}^{e,\langle 110\rangle}_{\text{stress}} = A\sigma + \tfrac{1}{2}\eta\sigma(3l_z^2 - 2) + \sqrt{\tfrac{1}{3}}\gamma\sigma T_{xy} \tag{3.10}$$

where, in principle, the parameters η and γ should be exactly the same as those defined in equations (3.8) and (3.9). (We note that both parameters have also absorbed the appropriate JT reduction factors.)

3.2.2. The vibronic ground state. The ground state is simpler to model as spin–orbit coupling has no matrix elements within an E orbital doublet and thus there is no equivalence of (3.5) and (3.6) for this state. The effective random 'strain' is assumed to have a fixed value as in the excited state and thus can be written as

$$\mathcal{H}^{g}_{\text{strain}} = \alpha' T_1. \tag{3.11}$$

For stress along $\langle 001\rangle$, we have

$$\mathcal{H}^{g,\langle 001\rangle}_{\text{stress}} = \Xi\sigma T_1 \tag{3.12}$$

and for stresses along $\langle 111\rangle$ and $\langle 110\rangle$, we have

$$\begin{aligned} \mathcal{H}^{g,\langle 111\rangle}_{\text{stress}} &= 0 \\ \mathcal{H}^{g,\langle 110\rangle}_{\text{stress}} &= -\tfrac{1}{2}\Xi\sigma T_1 \end{aligned} \tag{3.13}$$

respectively, where α' and Ξ are coefficients to be determined.

3.2.3. Second-order effects. In addition to the first-order terms given above, second-order stress terms should also be considered. They are of three types; the first and probably most important arises from stress along the $\langle 111\rangle$ or $\langle 110\rangle$ axis which couples the ^{2}E ground vibronic states to the excited vibronic ^{2}T$_2$ state. (Stress along $\langle 001\rangle$ does not couple the ^{2}E and ^{2}T$_2$ vibronic states and thus does not give any contribution.) The second type of contribution originates from the JT effect itself and involves second-order JT reduction factors involving the stress taken twice in a standard perturbation formalism and the third type arise from quadratic coupling.

Contributions from the first type may be described by the general Hamiltonian [24]

$$\mathcal{H}^{\text{E}-\text{T}_2}_{\text{stress}} = W[\bar{Q}_4\tau_x + \bar{Q}_5\tau_y + \bar{Q}_6\tau_z] \tag{3.14}$$

where

$$\tau_x = L_y L_z + L_z L_y \qquad \text{etc} \tag{3.15}$$

and where L_x etc is the orbital operator belonging to $l = 2$ etc, W is the effective coupling constant and $\bar{Q}_4$ etc is the static displacement of the Q_4 mode caused by the stress. As noted earlier, spin–orbit coupling also couples together the ^{2}E and ^{2}T$_2$ states separated by Δ. On projecting both stress and spin–orbit coupling into the ^{2}E state, three second-order contributions arise. One involves the spin–orbit coupling twice, but this causes no splittings and can be dropped. The second involves the stress twice and the third contribution is the cross term. On neglecting the second t$_2$-type terms involving $\bar{Q}_7$, $\bar{Q}_8$ and $\bar{Q}_9$ (because they give no extra information), the second-order effective Hamiltonian to be included then becomes

$$\begin{aligned}\mathcal{H}^{g(2)}_{\text{stress}} = {} & d[S_x\bar{Q}_4 + S_y\bar{Q}_5 + S_z\bar{Q}_6]T_3 + W_2[(2\bar{Q}_6^2 - \bar{Q}_4^2 - \bar{Q}_5^2)T_1 + \sqrt{3}(\bar{Q}_4^2 - \bar{Q}_5^2)T_2] \\ & + \tfrac{1}{2}e[\bar{Q}_4^2 + \bar{Q}_5^2 + \bar{Q}_6^2]l(l+1)\end{aligned} \tag{3.16}$$

where

$$\begin{aligned} d &= -4W\lambda/\Delta \\ W_2 &= e = W^2/(2\Delta) \\ T_3 &= \tfrac{1}{2}\mathrm{i}[|\theta\rangle\langle\epsilon| - |\epsilon\rangle\langle\theta|]. \end{aligned}$$

Further simplification occurs because, for a $\langle 111\rangle$ stress, $\bar{Q}_4 = \bar{Q}_5 = \bar{Q}_6 = Q_0$, so the final second-order effective Hamiltonian is

$$\mathcal{H}^{g(2)}_{\langle 111\rangle} = d'\sigma[S_x + S_y + S_z]T_3 + e'\sigma^2 \tag{3.17}$$

where the parameters d' and e' absorb JT reduction and other conversion factors including Q_0 and the term in W_2 drops out. We note the appearance of the term in σ^2 which does not involve any orbital or spin operators. For a $\langle 110\rangle$ stress, $\bar{Q}_4 = \bar{Q}_5 = 0$ and $\bar{Q}_6 = 3Q_0/2$ and the effective Hamiltonian is

$$\mathcal{H}^{g}_{\langle 110\rangle} = 3d'\sigma S_z T_3/2 + 3e'\sigma^2/4 + 9W_2'\sigma^2 T_1/2. \tag{3.18}$$

A similar procedure must be adopted for the orbital triplet. Thus the additional second-order contribution to the final effective Hamiltonian is

$$\begin{aligned}\mathcal{H}^{e(2)}_{\langle 111\rangle} = {} & G_1\sigma^2 + G_2\sigma^2(T_{yz} + T_{zx} + T_{xy}) \\ & + G_3\sigma[(\boldsymbol{l}\cdot\boldsymbol{s})(T_{yz} + T_{zx} + T_{xy}) + (T_{yz} + T_{zx} + T_{xy})(\boldsymbol{l}\cdot\boldsymbol{S})]\end{aligned} \tag{3.19}$$

where the parameters G_1, G_2 and G_3 include JT reduction and other conversion factors. (Note that those from the spin–orbit coupling taken twice have already been given in (3.6).) For the $\langle 110\rangle$ stress, a similar result is obtained, namely

$$\mathcal{H}^{e(2)}_{\langle 110\rangle} = \tfrac{3}{4}G_1'\sigma^2 + 3G_3\sigma[(\boldsymbol{l}\cdot\boldsymbol{s})T_{xy} + T_{xy}(\boldsymbol{l}\cdot\boldsymbol{S})]/2 - 3G_1\sigma^2 E_\theta/2 \tag{3.20}$$

where G_1' is another parameter.

As mentioned above, the second type of second-order contributions arise entirely from the JT effect. Details of this theory and the results obtained for an orbital triplet are given in [25] and for an orbital doublet in [26]. The additional non-zero Hamiltonians to be added, in an obvious notation, may be summarized as follows:

(i) for stress along $\langle 001\rangle$,

$$\begin{aligned}\mathcal{H}^{(2)g,\langle 001\rangle}_{\text{stress}} &= -\Xi_2\sigma^2 T_1 \\ \mathcal{H}^{(2)e,\langle 001\rangle}_{\text{stress}} &= \tfrac{1}{4}[3\xi_1 l(l+1) - 2\xi_2 E_\theta]\sigma^2\end{aligned} \tag{3.21a}$$

(ii) for stress along ⟨110⟩,

$$\mathcal{H}_{\text{stress}}^{(2)e,\langle 110\rangle} = -\tfrac{3}{4}\zeta_1 T_{xy}\sigma^2 \tag{3.21b}$$

where Ξ_2, ξ_1, ξ_2 and ζ_1 are parameters. There are also second-order JT contributions from the ⟨111⟩ stress but these contributions may be absorbed into (3.17) and (3.19) by changing the definitions of the parameters. (We neglect the corresponding second-order contributions from 'strain'.)

The third type of contribution arise from quadratic and bi-linear couplings in the basic JT system. Many of the corresponding terms have the same form as those already introduced (and are responsible for the differences between what would otherwise be identical parameters) but there are, in addition, two terms which were not included previously in the case of a ⟨110⟩ stress. Thus to the above expressions given in (3.21) we need to add

$$\begin{aligned}\mathcal{H}_{\text{stress}}^{(2)e',\langle 110\rangle} &= \zeta_2' E_\theta \sigma^2 \\ \mathcal{H}_{\text{stress}}^{(2)g',\langle 110\rangle} &= Z' T_1 \sigma^2\end{aligned} \tag{3.22}$$

where ζ_2' and Z' are new parameters. These parameters are combined with those obtained previously to generate the terms $\zeta_2 E_\theta \sigma^2$ and $Z T_1 \sigma^2$ in the effective Hamiltonians for the excited and ground states respectively, where

$$\begin{aligned}\zeta_2 &= \zeta_2' - 3G_1/2 \\ Z &= Z' + 9W_2'/2.\end{aligned} \tag{3.23}$$

3.3. The transition intensities

In optical experiments, transitions occur between vibronic states. Although the absolute intensities of the dominant electric-dipole transitions are difficult to calculate, because they depend upon the amount of wave-function mixing with other free-ion and odd-parity states and on the poorly known radial parts of the wave functions, the relative intensities can be deduced accurately because they rely heavily on symmetry arguments. Thus the transition intensities are proportional to the square of the matrix elements of the operator $H(p)$ between the 3d components of the ground and excited states where $H(p)$ is given by

$$H(p) = E_x T_{yz} + E_y T_{zx} + E_z T_{xy} \tag{3.24}$$

and where E_x etc are the components of the electric field (of symmetry T_2 for a T_d site) of the radiation field.

Unfortunately, there are many modifications which should be made to the above intensity calculations because strain effects make a significant contribution to the shape of the OA spectrum. If we have a static situation in the strong-coupling limit, strain will shift the relative energies of the wells in the potential energy surface. However, in order to build up a line-shape for OA, ideally the strain distribution function should be incorporated. However, this is very complicated and thus, in order to simplify the calculations, we neglect the broadening effects from strain and concentrate on the position and sizes of the peaks themselves. Also we assume that the peak corresponds to a fixed finite size of strain.

4. The results of computer fitting

The procedure adopted was to obtain values for the parameters from the peak energy positions only as a function of applied stress for all stress directions, and to use these

Table 2. Values obtained for the parameters. (Note that $G' = G_1 - e'$ and $G'' = G_1' - e''$.)

Parameters	$\boldsymbol{P}\|[001]$	$\boldsymbol{P}\|[111]$	$\boldsymbol{P}\|[110]$
α (cm^{-1})	0.57	0.57	0.57
α' (cm^{-1})	−0.4	−0.4	−0.4
Ξ (cm^{-1} MPa^{-1})	−0.152		−0.152
η (cm^{-1} MPa^{-1})	6.19×10^{-2}		6.19×10^{-2}
A (cm^{-1} MPa^{-1})	1.17×10^{-2}	1.17×10^{-2}	1.17×10^{-2}
γ (cm^{-1} MPa^{-1})		-5.63×10^{-2}	-5.63×10^{-2}
d' (cm^{-1} MPa^{-1})		1.57×10^{-2}	1.57×10^{-2}
G_3 (cm^{-1} MPa^{-1})		6.73×10^{-4}	6.73×10^{-4}
ξ_1 (cm^{-1} MPa^{-2})	-5.65×10^{-5}		*
ξ_2 (cm^{-1} MPa^{-2})	5.80×10^{-4}		
G' (cm^{-1} MPa^{-2})		-1.33×10^{-4}	*
G_2 (cm^{-1} MPa^{-2})		2.50×10^{-5}	
G'' (cm^{-1} MPa^{-2})			-1.69×10^{-4}
ζ_1 (cm^{-1} MPa^{-2})			1.12×10^{-5}
ζ_2 (cm^{-1} MPa^{-2})			-1.89×10^{-5}
Z (cm^{-1} MPa^{-2})			-7.93×10^{-5}
Ξ_2 (cm^{-1} MPa^{-2})	1.46×10^{-5}		1.46×10^{-5}

* The parameter has some contribution in the direction, but its effect is combined into other parameters.

values to predict the intensities of the various theoretical peaks. The quality of a given fit was therefore judged by comparing the calculated peak positions and the predicted intensities with the corresponding experimental values as given in figures 1–3 and 5–7 and summarized in table 1.

4.1. The values of the parameters

In principle, the energy levels for the Ti^{3+} ion are obtained directly from $\mathcal{H}^e_{eff}$ and $\mathcal{H}^g_{eff}$ with substitution of the appropriate spin–orbit coupling, strain and all of the stress Hamiltonians. In general, the energy levels are split in the schematic way shown in figure 4 but the identification of an observed peak with a given transition is not always obvious and part of the problem is to correlate the two in a consistent way.

In order to obtain an initial fit, the data were divided into four sets, all in zero magnetic field, namely the zero-stress spectrum and the spectra for $\boldsymbol{\sigma}$ along $\langle 001 \rangle$, $\langle 111 \rangle$ and $\langle 110 \rangle$ successively. It was found that some parameters were much more precisely determined from one set of data than from other sets. Consequently, numerous computer fits were undertaken using various combinations of the four sets of data and by a variety of computer routines to produce a self-consistent set of transition energies and relative intensities using the theory outlined in section 3 and parameter values for each particular combination of data. These procedures proved unreliable due to the multi-dimensional character of the problem. Finally, an alternative procedure was adopted in which the zero-order (i.e. involving α and α') and linear stress terms only (i.e. those involving the parameters d', Ξ, η, A and γ) were used in a hands-on best fit to all of the stress data. (It should be noted that the sign of the ground-state parameter Ξ was determined unambiguously by comparing the calculated and observed intensities.) Then the remaining first-order parameter G_3 and the second-order parameters G' $(=G_1 - e')$, G'' $(=G_1' - e'')$, Ξ_2, ξ_1, ξ_2, ζ_1, ζ_2 and Z were added and the fit was improved with the former first-order parameters remaining unchanged. (Note also that only the difference between the stress-independent parameters G_1 and e' could be obtained

and hence the introduction of G'.) The best fit which was obtained by these processes is shown in table 2 grouped together under a particular stress direction in which the parameter has an effect.

Table 3. The calculated relative intensities for $\boldsymbol{\sigma}$ along $\langle 001 \rangle$ for $\sigma = 15$ MPa.

Transitions	1	2	3	4	5	6
$\boldsymbol{E} \parallel \boldsymbol{\sigma}$	0	3.27	0	0	8.27	0
$\boldsymbol{E} \perp \boldsymbol{\sigma}$	1.5	1.09	2.36	1.72	0.409	0.646
Unpolarized	3.0	5.45	4.73	3.44	9.54	1.29

Table 4. The calculated relative intensities for $\boldsymbol{\sigma}$ along $\langle 111 \rangle$ for $\sigma = 100$ MPa.

Transitions	1	2	3	4	5	6
$\boldsymbol{E} \parallel \boldsymbol{\sigma}$	4.26	12.52	10.906	3.095	1.207	0.473
$\boldsymbol{E} \perp \boldsymbol{\sigma}$	4.52	1.283	1.762	5.63	0.196	7.083
Unpolarized	4.123	6.574	6.334	4.362	7.301	3.77

The theoretical energy–stress curves calculated from these parameters are shown in figures 5–7 together with the corresponding experimental points for the three stress directions. Agreement between the calculated curves and experimental data is within the experimental uncertainty. Peak intensities for specific values and directions of the uniaxial stress have been calculated also and the results are given in tables 3 and 4. These results are qualitatively in reasonable agreement with the experimental results (e.g. figures 2 and 3) bearing in mind the simplifications used in the initial calculations through the total neglect of the random strain distribution function in our calculations.

4.2. Discussion

We now examine in more detail the spectra shown in figures 2 and 3 concentrating on those spectra for which polarized light was used. For $\boldsymbol{\sigma}$ directed along $\langle 001 \rangle$ and of magnitude 15 MPa and $\boldsymbol{E}$ along $\boldsymbol{\sigma}$, figure 2(c) shows clearly that the strongest line is line 5 and that line 2 is the next strongest. For $\boldsymbol{E}$ perpendicular to $\boldsymbol{\sigma}$, lines 5 and 6 are clearly the weakest (figure 2(b)), line 1 is stronger than line 2 and line 3 is stronger than line 4. However, it is more difficult to compare lines 1 and 3 because of their different widths. In principle, we need to calculate the area of the absorption and not just the peak height and this involves an estimate of the position of the base-line. When such an analysis is undertaken, we see experimentally that the strongest line is line 3. Thus, in all cases, the theoretical intensities given in table 3 are in general agreement with the experimental values. Very similar comments can be made for the results obtained for $\boldsymbol{P}$ along $\langle 111 \rangle$ and along $\langle 110 \rangle$. Details are given in Al-Shaikh [27]. In all cases it appears that the calculated and experimental intensities are in reasonable agreement with one another.

Despite the approximations involved in calculating the various intensities of the lines, the theoretical intensities follow closely those seen in the experiments in all cases where the spectra are well defined, both for different values of σ and for differing geometries, and that the revised energy level scheme of figure 4 adequately explains all of the stress data. It is also clear that the parameter values satisfy the requirement that first-order terms

are significantly larger than second-order terms with the one exception of the spin–orbit coupling/stress term involving d'. This latter result is expected because the spin–orbit coupling is larger than the effects of stress.

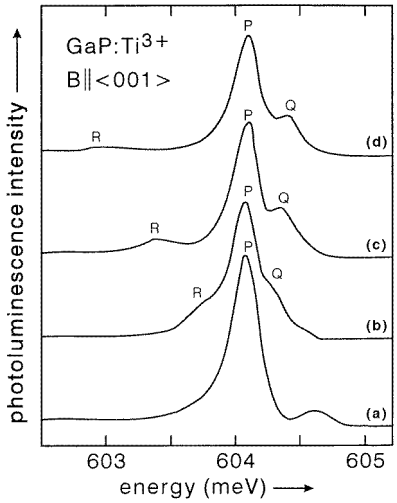

Figure 9. Photoluminescence spectra of GaP:Ti^{3+} measured at $T = 2$ K with the magnetic field $\boldsymbol{B}$ along the $\langle 001 \rangle$ direction. (a) $B = 0$, (b) $B = 3$ T, (c) $B = 6$ T, (d) $B = 9.3$ T (after [18]).

5. Zeeman effect results reinterpreted with the Jahn–Teller model

5.1. Summary of the Zeeman data

The lines at 4873.0 cm^{-1} and 4876.3 cm^{-1} in GaP:Ti^{3+} were also observed previously in PL experiments [17]. Zeeman effect experiments on these samples were reported earlier [18] using magnetic fields B up to 9.3 T. Figure 9 gives the PL spectrum showing the three main peaks labelled P, Q and R for four values of a magnetic field $\boldsymbol{B}$ along $\langle 001 \rangle$. Figure 10 shows the Zeeman splittings as a function of $\boldsymbol{B}$ directed along $\langle 001 \rangle$, $\langle 111 \rangle$ and $\langle 110 \rangle$. All of the measurements were carried out at 2 K. While the qualitative interpretation of the results proposed in [18] remains correct (namely that the lines P and R are the transitions from the lowest Zeeman level of the excited $\Gamma_8(^2T_2)$ state to the $m_s = -\frac{1}{2}$ and $m_s = +\frac{1}{2}$ Zeeman levels of the $\Gamma_8(^2E)$ ground state), the details have to be reinterpreted starting from the revised energy level scheme of figure 4 for $\sigma = 0$ and $B = 0$. In particular, the above comment concerning the P and R lines is clearly correct as, at high magnetic fields and for $T = 2$ K, only the lowest Zeeman level of the excited state is populated. Therefore, we use the JT model developed in section 3 to describe the effect of a magnetic field on the $^2E \leftrightarrow {}^2T_2$ transitions.

5.2. The Zeeman effective Hamiltonians

For the vibronic excited state, including all first- and second-order JT contributions, the extra terms arising from the magnetic field $\boldsymbol{B}$ generate the additional effective Hamiltonian

$$\mathcal{H}_B^e = \mu_B\big[\boldsymbol{B}\cdot(a'\boldsymbol{l} + 2\boldsymbol{S}) + e(\boldsymbol{B}\cdot\boldsymbol{S}) + 2c(E_\theta E_\theta^{SB} + E_\epsilon E_\epsilon^{SB}) + b[(\boldsymbol{l}\cdot\boldsymbol{S})(\boldsymbol{l}\cdot\boldsymbol{B}) + (\boldsymbol{l}\cdot\boldsymbol{B})(\boldsymbol{l}\cdot\boldsymbol{S})]\big] \tag{5.1}$$

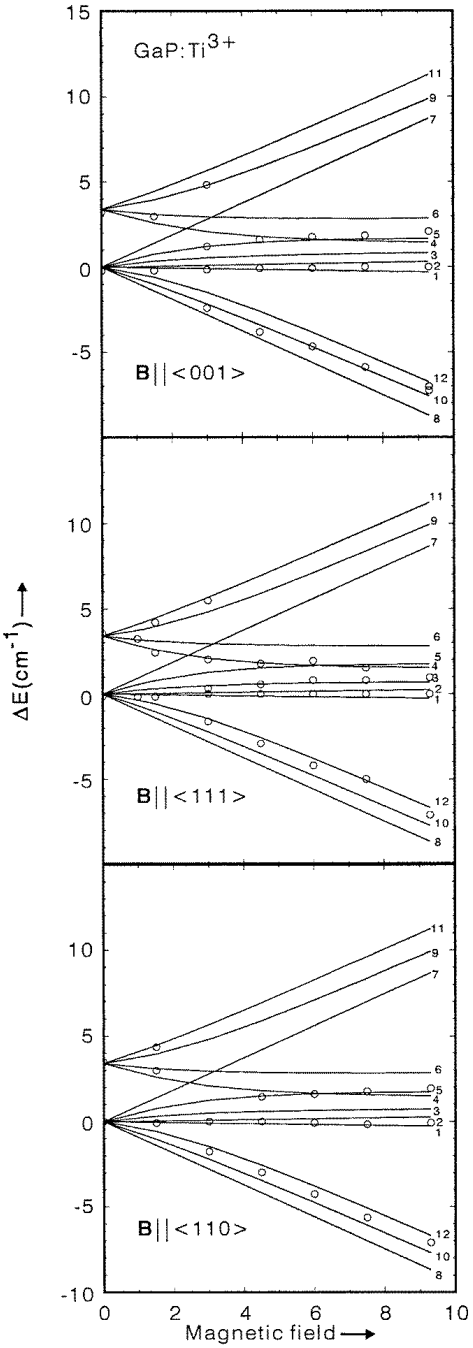

Figure 10. Splittings and shifts of the photoluminescence lines due to the $^2T_2 \rightarrow {}^2E$ transitions of Ti^{3+}_{Ga} in GaP with the magnetic field $\boldsymbol{B}$ applied along the ⟨001⟩, ⟨111⟩ and ⟨110⟩ directions measured at $T = 2$ K. The circles are the measured line positions with $\Delta E = 0$ at 4873.0 cm^{-1} (after [18]). The curves are calculated with the parameters given in section 7; the numbers indicate the transitions between the Zeeman levels according to the level scheme of figure 11.

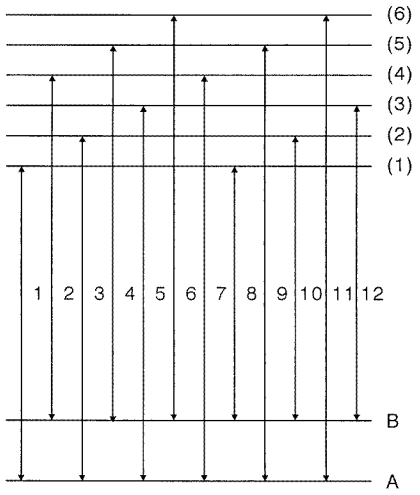

Figure 11. The schematic energy level pattern defining the Zeeman transitions.

where μ_B is the Bohr magneton and where

$$E_\theta^{SB} = \tfrac{1}{2}[2B_z S_z - \boldsymbol{B}\cdot\boldsymbol{S}] \qquad \text{etc.} \tag{5.2}$$

The form of the above Hamiltonian closely resembles that of the spin–orbit coupling alone (equation (3.6)).

For the vibronic ground state, the corresponding Hamiltonian is of the form

$$\mathcal{H}_B^g = g_\parallel \mu_B B_z S_z + \tfrac{1}{2} g_\perp \mu_B (B_+ S_- + B_- S_+) \tag{5.3}$$

where $g_\parallel$ and $g_\perp$ are the effective g-values as the orbital contributions are very small. Using the parameter values deduced above (table 2) together with the measured g-values [10]

$$g_\parallel = g_\perp = 1.943 \pm 0.003$$

from EPR experiments, the theoretical transitions can be computed directly for all values of the magnetic field and compared directly with the experimental data shown in figure 10. For ease of reference, the predicted transitions will be labelled 1–12 according to the scheme shown in figure 11. The label P corresponds to transitions 1, 2, 3, 4, 5 and 6, label R to transitions 8, 10 and 12 and label Q to transitions 7, 9 and 11. Further calculations have shown that the spectra are almost isotropic as the magnetic field is rotated about the z-axis in agreement with experiment [18].

5.3. The transition probabilities

The transition probabilities have also been calculated by the same procedure as that used previously. The only difference is that, in PL experiments, the effective temperature of the excited states is uncertain. (It was also noted that the relative intensities were observed to be power dependent). Thus the Boltzmann factor was included for transitions other than those from the lowest level. The experimental results were complicated by the 'hot' components interfering with 'cold' components which further obscured the picture.

5.4. Discussion

Figures 10 clearly show that the original P, Q and R lines, such as those shown in figure 9, are really the convolution of several components which form into these three sets. Further calculations [28] show that the components have different intensities. Also, our model retains the virtually field-independent nature of the P and Q lines noted first by Halliday *et al* [18]. Our analysis has also shown that the separation into the various sites having symmetry axes O_x, O_y and O_z as developed in [18] has much less importance in our revised model. Instead, each main peak in the Zeeman spectra consists of contributions from all Ti^{3+} ions.

6. Conclusions

The revised level scheme shown in figure 4 for zero stress and zero magnetic field together with the effective Hamiltonians derived in Section 3 gives a good description of the new uniaxial stress data for the GaP:Ti^{3+} system as described in section 2. The same model is also shown to give a good description of published Zeeman data. This model represents a complete revision of the scheme for the Ti^{3+} ion in GaP. It is also expected that the GaAs:Ti^{3+} and InP:Ti^{3+} systems would behave in exactly the same way (with different values for the parameters) but such an analysis falls outside the scope of the present paper and equivalent experimental data would be required.

The GaP:Ti^{3+} system is of considerable interest from a theoretical point of view. First, we note that we have needed to introduce some small 'strain'-like splittings having a specific magnitude in both the ^2E ground and $^2T_2$ excited states. The reason for this is unclear but similar terms are needed in the case of Cr^{3+} impurities in GaP [28].

In addition to the understanding of these effective strains, this system is ideal in many respects for the study of the nature of the vibronic couplings involved in the excited state. There is no direct evidence from experiment that the orthorhombic $T \otimes (e + t_2)$ JT effect is operational unlike the case of the GaAs:Cr^{3+} system for which the angular dependence of the EPR spectrum from the $^4T_1$ ground state in that system (GaAs:Cr^{3+}) clearly showed that the Cr^{3+} ion occupies a site with orthorhombic symmetry [29, 30]. The fact that the GaP:Ti^{3+} system is affected by both e- and t_2-type stresses is not in itself sufficient to allow us to make the assumption that the system is an orthorhombic JT system. Instead, the formalism above for the vibronic triplet encompasses coupling to the e and two t_2 modes simultaneously. It does not assume that it is an $E \otimes e$ or $T \otimes (e + 2t_2)$ system. It also includes the possibility of a mixed JT system in which there is approximately equal coupling to both e and t_2 modes but without the orthorhombic-type wells being involved [31]. Further discussions and work on such a mixed system remain for future study.

Although Ti^{3+} initially appeared to be an ideal simple system to study, our analysis has become very complicated on account of the necessity to involve many different perturbations combined with JT effects for the GaP host. For example, it is impossible to deduce a value for the first-order reduction factor K to replace the value of 0.12 quoted originally in section 1 because the relevant parameter a' also contains inherently contributions from second order. It is also virtually impossible to obtain values for many of the other basic parameters from the results of table 2 because of the complicated way in which the various perturbations enter the final result. However, the final values given in table 2 appear to be self consistent with each other and fit in with expectations from the theory. This work clearly emphasizes the care needed in the study and identification of defect impurities even in cases which appear to be straightforward.

Acknowledgments

The authors wish to thank the late Dr A-M Vasson, and Dr A Vasson and colleagues for many helpful discussions on this topic. One of us (QCQ) wishes to thank the UK Committee of Vice-Chancellors and Principals for support from the Overseas Research Students Award Scheme.

References

[1] Hennel A M, Brandt C D, Ko K Y and Pawlowicz L M 1986 *Mater. Sci. Forum* **10–12** 645
[2] Bremond G, Guillot G, Nouailhat A, Lambert B, Toudic Y, Gauneau M and Deveaud B 1986 *Mater. Sci. Forum* **10–12** 657
[3] Guillot G, Bremond G, Bencherifa A, Nouailhat A and Ulrici W 1986 *Semi-Insulating III–V Materials (Tokyo)* ed H Kukimoto and S Miyazawa (Amsterdam: North-Holland) p 483
[4] Bremond G, Guillot G, Nouailhat A, Lambert B, Toudic Y, Gauneau M and Deveaud B 1986 *J. Phys. C: Solid State Phys.* **19** 4723
[5] Brandt C D, Hennel A M, Pawlowicz L M, Wu Y T, Bryskiewicz T, Lagowski J and Gatos H C 1986 *Appl. Phys. Lett.* **48** 1162
[6] Roura P, Bremond G, Nouailhat A, Guillot G and Ulrici W 1987 *Appl. Phys. Lett.* **51** 1696
[7] Brandt C D, Hennel A M, Bryskiewicz T, Cho K Y, Pawlowicz L M and Gatos H C 1989 *J. Appl. Phys.* **65** 3459
[8] Scheffler H, Korb W, Bimberg D and Ulrici W 1990 *Appl. Phys. Lett.* **57** 1318
[9] Bremond G, Guillot G, Roura P and Ulrici W 1986 *Semicond. Sci. Technol.* **6** 85
[10] Kreissl J, Ulrici W and Gehlhoff W 1988 *Phys. Status Solidi* b **150** K57
[11] Kreissl J, Ulrici W and Gehlhoff W 1989 *Phys. Status Solidi* b **155** 597
[12] Clerjaud B, Hennel A M and Brandt C D 1987 *Semicond. Sci. Technol.* **2** 65
[13] Kreissl J, Gehlhoff W and Ulrici W 1987 *Phys. Status Solidi* b **143** 207
[14] Ulrici W, L. Eaves L, Friedland K, Halliday D P, Nash K and Skolnick M S 1986 *J. Phys. C: Solid State Phys.* **19** L525
[15] Martini P H, Hennel A M, Aggarwal A L, Liro Z and Brandt C D 1988 *Semi-Insulating III–V Materials 1988* (Bristol: Hilger) p 355
[16] Hennel A M, Brandt C D, Wu Y T, Bryskiewicz T, Ko K Y, Lagowski J and Gatos H C 1986 *Phys. Rev.* B **33** 7353
[17] Ulrici W, Friedland K, Eaves L, Halliday D P and Payling C A 1988 *Phys. Status Solidi* b **150** 177
[18] Halliday D P, Payling C A, Saker M K, Skolnick M S and Ulrici W 1987 *Semicond. Sci. Technol.* **2** 679
[19] Clerjaud B 1985 *J. Phys. C: Solid State Phys.* **18** 3615
[20] Bates C A and Stevens K W H 1986 *Rep. Prog. Phys.* **49** 783
[21] Ham F S 1965 *Phys. Rev.* **138** A1727
[22] Dunn J L, Bates C A and Kirk P J 1990 *J. Phys.: Condens. Matter* **2** 10 379
[23] Hallam L D, Dunn J L and Bates C A 1992 *J. Phys.: Condens. Matter* **4** 6797
[24] Clerjaud B 1988 *Acta Phys. Pol.* A **73** 909
[25] Jamila S, Dunn J L and Bates C A 1992 *J. Phys.: Condens. Matter* **4** 4945
[26] Badran R I, Jamila S, Kirk P J, Bates C A and Dunn J L 1993 *J. Phys.: Condens. Matter* **5** 1505
[27] Al-Shaikh A M 1991 *PhD Thesis* University of Nottingham
[28] Dunn J L, Bates C A, Darcha M, Vasson A and Vasson A-M 1986 *Phys. Rev.* B **33** 2029
[29] Krebs J J and Stauss G H 1977 *Phys. Rev.* B **15** 17
[30] Parker L W, Bates C A, Dunn J L, Vasson A and Vasson A-M 1990 *J. Phys.: Condens. Matter* **2** 2841
[31] Liu Y M, Dunn J L and Bates C A 1995 *J. Phys.: Condens. Matter* **6** 7521